Experimental Study of Rectangular RC Columns Strengthened with CFRP Composites under Eccentric Loading

Pedram Sadeghian [1]; Ali R. Rahai [2]; and Mohammad R. Ehsani, M.ASCE [3]

Abstract

This paper presents the results of experimental studies on reinforced concrete columns strengthened with CFRP composites under combination of axial load and bending moment. A total of seven large-scale specimens with rectangular cross section (200 mm × 300 mm) were prepared and tested under eccentric compressive loading up to failure. The overall length of specimens with two haunched heads was 2700 mm. Different FRP thicknesses of 2, 3, and 5 layers, fiber orientation of 0^o, 45^o, and 90^o, and two eccentricities of 200 and 300 mm were investigated. The effects of these parameters on load-displacement and moment-curvature behavior of the columns as well as the variation of longitudinal and transverse strains on different faces of the columns were studied. The results of the study demonstrated significant enhancement on performance of strengthened columns compared to unstrengthened columns.

Keywords: CFRP; Concrete column; Eccentric loading; Strengthening; Fiber orientation; Rectangular section; Ductility.

[1] *Post Doctoral Fellow, Dept. of Civil Engineering, Queen's University, Kingston, ON, Canada K7L 3N6 (corresponding author). E-mail: P.Sadeghian@queensu.ca*

[2] *Professor, Dept. of Civil and Environmental Engineering, Amirkabir University of Technology, Tehran, Iran. E-mail: Rahai@aut.ac.ir*

[3] *Professor, Dept. of Civil Engineering and Engineering Mechanics, University of Arizona, Tucson, AZ 85721, USA. E-mail: Mo@QuakeWrap.com*

Introduction

The use of externally applied fiber reinforced polymer (FRP) composites has gained significant popularity for the strengthening and repair of concrete structures. FRP composites have been used successfully for strengthening of deficient reinforced concrete structures including bridges and buildings. Concrete columns in these structures are essential elements that may need to be strengthened. In recent years, several studies have been conducted about FRP confined and strengthened columns under concentric loads. However, it is clear that most columns are loaded under combination of axial compression load and bending moment (i.e. eccentric compression loading). So there is a need for research on behavior of FRP strengthened columns under eccentric loading. The present paper is a step along this direction.

Some research has been conducted on FRP confined columns under eccentric loading. In a study performed by Parvin and Wang (2001), small-scale square concrete columns (i.e. 108 mm × 108 mm × 305 mm) were strengthened with varying layers of carbon FRP (CFRP) composites and tested subjected to axial load at different eccentricities. The eccentric loading was achieved by placing a knife edge at a set distance from the centre of the cross section of the column. The results showed that the increase in eccentricity resulted in a decrease in strength capacity of the column, and the use of CFRP increased the load capacity of the column.

Yuan et al. (2001) performed a comparative study of concrete stress-strain models and applied these models for FRP confined reinforced concrete (RC) columns under combined bending and compression and axial load-bending moment interaction curves (P-M interaction curves) were presented. In another research, Fam et al. (2003) performed an experimental program and proposed an analytical model to describe the behavior of concrete filled FRP tubes subjected to combined axial compression loads and bending moments. The

experimental program included 10 specimens subjected to eccentric axial loads, two specimens tested under concentric axial loads, and two specimens tested in bending. Glass FRP (GFRP) tubes with two different laminate structures were considered and P-M interaction curves were presented.

Li and Hadi (2003), Hadi and Li (2004), and Hadi (2006a,b; 2007a,b) tested several FRP-strengthened concrete columns with circular section under eccentric loading at different conditions. The specimens were haunched at either one end or both ends. The effects of concrete strength, internal steel reinforcement, wrap type, fiber orientation, and eccentricity were studied. The eccentric load was applied through a circular plate at each haunched ends of the specimens. The experimental results clearly demonstrated that the FRP wrapping can enhance strength, ductility, and energy absorption of circular concrete columns under eccentric loading.

In a study performed by Chaallal and Shahawy (2000), an experimental investigation was conducted on rectangular RC beam-columns strengthened with bidirectional CFRP composites and different eccentricities. The overall length of the two haunched-head specimens was 3.6 m (200 mm wide and 350 mm high in test section). The results indicated that the strength capacity of beam-columns improved significantly as a result of the combined action of the longitudinal and the transverse fibers of the bidirectional composite fabrics and P-M curves were presented.

Lignola et al. (2007) have mainly focused their attention on square hollow columns strengthened with CFRP composites (height of 3020 mm, width of 360 mm, and wall thicknesses of 60 mm). A total of seven RC specimens with haunched solid head were prepared, wrapped in transverse direction, and tested under various eccentric loading. The outcomes highlighted that composite wrapping can enhance the structural performance of concrete columns under eccentric loading in terms of strength and especially in terms of

ductility. The strength improvement was more pronounced in the case of specimens loaded with smaller eccentricity, while the ductility improvement was more significant in the case of larger eccentricity.

Research Significance

According to the previous researches on the subject, there are a number of issues that need to be addressed: (1) Behavior of FRP strengthened RC columns under eccentric loading is not well known. So this subject needs more research. (2) Little information is available on the rectangular sections because most studies have concentrated on circular sections. (3) In eccentric loading, longitudinal fibers have essential significant effect on flexural behavior, while transverse fibers increase axial strength and ductility of column through lateral confinement. So fiber orientation and configuration of the layers of FRP reinforcement require more investigation.

The present experimental study focuses on behavior of strengthened RC columns with unidirectional CFRP composites under eccentric loading. A number of large-scale specimens with different fiber orientations were prepared and tested under two eccentricities. The findings of this study will be of interest to those engineers involved in retrofit and strengthening of structures with FRP materials.

Experimental Program

Specimen Layout

A total of seven RC specimens were designed with rectangular section (200 mm × 300 mm). The test portion of each specimen had a height of 1500 mm and each haunched head had a height of 600 mm. The specimens were tested under compression eccentric loading up to

failure. The corners of cross section were chamfered to a radius of 15 mm. Fig. 1 shows the geometry of the specimens.

Main experimental parameters were FRP thickness, fiber orientation, and eccentricity. Three different FRP thicknesses of 1.8, 2.7, and 4.5 mm (2, 3, and 5 layers), four fiber orientation of 0^o, 90^o, $+45^o$, and -45^o with respect to an axis perpendicular to the column axis, and two eccentricities of 200 and 300 mm were investigated. The test program and specimen properties are summarized in Table 1, where L refers to an FRP layer whose axis is parallel to the column axis (90^o), T refers to an FRP layer whose axis is perpendicular to the column axis and is used for lateral confinement of the column (0^o), D is the diagonal direction ($+45^o$), and D' is the inversed diagonal direction ($+135^o$ which is the same as -45^o). The 90^o (i.e. L) layers were applied as a longitudinal external (flexural) strengthening with continuous strips along the columns axis. All layers (i.e. longitudinal, transverse, and diagonal) were applied as uniaxial strips to cover all faces of the specimens, consistently.

The specimens were divided into two groups. The first group, labeled "S", consisted of strengthened specimens, and the second group labeled "U", were unstrengthened and served as control specimens. Two columns were unstrengthened, two were strengthened with two longitudinal layers and one transverse layer of CFRP (L2T), two other were strengthened with four longitudinal layers and one transverse layer of CFRP (L4T), and the last column was strengthened with two diagonal layers of CFRP (DD'). One specimen of each group was tested under eccentricity of 200 mm, and another was tested under eccentricity of 300 mm. The specimen DD' was tested under an eccentricity of 300 mm only.

Material Properties

All specimens were cast from one batch of concrete with a 28-day compressive strength of f_c' = 40 MPa and a slump of 80 mm. All specimens were reinforced with 4Φ12 mm

longitudinal ribbed bars (f_y = 465 MPa), symmetrically placed. Transverse reinforcement was provided with rectangular ties Φ6.5@200 mm made of smooth bars (f_y = 325 MPa). The clear concrete cover for the ties was 20 mm. The reinforcement details for the specimens are shown in Fig. 1. Extra longitudinal and transverse reinforcement was provided in haunched heads in order to prevent premature failures. Unidirectional carbon fiber sheets were adopted. Mechanical properties of CFRP wraps through tension testing on CFRP coupons have been measured by Sadeghian et al. (2008). The average test results in longitudinal and transverse direction are shown in Table 2.

Specimen Preparation

The concrete was placed in one batch and cast in special steel formwork. After curing in humid condition for 28 days, the surface of specimens was cleaned and prepared for strengthening. In order to prevent anchorage rupture in transverse layers, a lap splice equal to 75 mm was used in fiber direction at mid length of the rectangular section. Longitudinal and diagonal layers were applied on full length of the specimens and anchored by extra transverse strips at the both ends of the prismatic part and haunched heads, as shown in a photograph of a strengthened specimen in Fig. 1. All of orientations are shown in this photograph, schematically.

The carbon fiber sheet was cut and impregnated with epoxy resin using the wet lay-up technique. The mixing ratio of the epoxy resin components was 100:15 by weight and resin was mixed for three minutes. The carbon fabric layers were each saturated with resin and placed in predefined orientations. The resin content was sufficient to ensure that subsequent layers of fabric would bond together. The layers were applied on all faces of the specimens and the layers with transverse fibers were the last layers. The epoxy resin cured at laboratory temperature (i.e. 22 $^{\circ}$C) for a minimum of seven days.

Test Setup and Loading

A hydraulic actuator was used to apply the axial load to the columns (Fig. 2). The upper ends of the specimens were attached to the actuator, while the lower ends were supported on the steel reaction frame. Both end supports were designed as hinged connections with predefined eccentricity. For this purpose a rectangular steel frame (200 mm × 600 mm) from an angle section member (L30×3 mm) was prepared for each end of the specimen and a roller welded to the frame at the predefined eccentricity.

The lateral stability of each specimen in and out of plane was maintained by appropriate steel supports, as shown in Fig. 2. In order to maintain out of plane stability, two long members with angle section (L120×12 mm) were applied on each face of the upper end of the specimen and bolted to the steel reaction frame as well as bolted to each other at almost each one meter distance. In case of in plane stability, one of the bolts was just contacted with the tension side of the upper head and the opposite face anchored to the reaction frame by a tight chain, as shown in Fig. 2. For the lower end of specimen, two supports were provided which contacted to the both faces of the specimen and welded to the base plates.

A total of six linear variable displacement transducers (LVDTs) and 26 strain gauges were used for every specimen. Fig. 3 shows the arrangement of LVDTs and strain gauges. The specimens were tested using a 600 kN capacity compression actuator under displacement control and the data were monitored using an automatic data collecting system. Displacements and strains were monitored by a digital data logger system. The tests were performed up to failure of the specimens. Force, displacements, and strains were obtained during the test and were filed by computer software. The test was stopped when the FRP failed on the tension face (i.e. for the strengthened specimens) or the concrete crushed on the

compression face (i.e. for the unstrengthened specimens), because the test setup and actuator situation were very sensitive and were not able to manage large post peak deformations.

Experimental Results and Discussions

Overall Behavior

The overall behavior was similar for all the strengthened specimens. At the early stages of loading of the strengthened specimens, the noise related to the micro cracking of concrete and stretch of the FRP was obvious, indicating the start of stress transfer from the concrete to the FRP. Prior to the failure, noises of the stretched FRP were extremely heard and curvature of specimen was visible. The maximum lateral deflection was almost seen at mid height of the specimen. The lateral deflection was gradual and no debonding took place between the FRP and the concrete during the tests. This behavior would end with a sudden rupture of the longitudinal (or diagonal in DD') layers on tension face of the specimen.

The rupture of the FRP was almost initiated at mid height of the specimens. At this time an impact was induced in the specimen with sudden increase of lateral deflection and decrease of load. The strength of all strengthened specimens increased significantly, but the post-peak behavior showed a sudden drop in both strength and stiffness. After the rupture of the FRP, concrete cracking progressed to both ends of the specimen. The sudden failure indicates the release of extraordinary amount of energy as a result of the tensile stress provided by the FRP. Inspection of the failed specimens showed yielding of longitudinal steel bar in tension face and buckling of longitudinal steel bar in compression face of the columns. In the –L2T and –L4T series specimens, whose final layer of FRP consisted of carbon fibers in the transverse direction, the bond between the longitudinal layers of FRPs and the bond between these layers and concrete improved. In the same specimens, the presence of lateral confinement led to better anchorage of the longitudinal layers.

The overall behavior of the unstrengthened specimens was typical. Tensile cracks were produced on tension face at the early stages of loading and propagated with increasing of loading. The cracks on mid height of the specimen were opened extensively when the tensile steel bars were yielded. The load dropped when the concrete on the compression face crushed and the compressive steel bars buckled. Fig. 4 shows the failure region of strengthened and unstrengthened specimens.

Load-Displacement Behavior

The load-displacement curves of the specimens with 300 mm eccentricity are shown in Fig. 5(a). The longitudinal displacement U_{Lon} was measured from the actuator displacement gauge and the lateral displacements U_{Lat} was obtained from the mid height LVDT. The unstrengthened specimen U300 has an approximate linear load-longitudinal displacement behavior up to yield point (i.e. Y), that steel bars on the tension face are yielded at a force of 128 kN and longitudinal and lateral displacement of 6.5 mm and 7.5 mm, respectively. The yielding point was evaluated when the load-displacement curve slope changes. The longitudinal secant stiffness is equal to 19.7 kN/mm. After the yield point, the stiffness is enormously decreased and plastic hinge is created. The plastic region has a small constant longitudinal tangent stiffness (i.e. 1.8 kN/m) due to the strain hardening of the steel bars. This bilinear behavior is continued up to concrete crushing and buckling of steel bars on the compression face of plastic hinge at a force of 156 kN and longitudinal displacement of 22.0 mm.

All strengthened specimens exhibited a similar bilinear behavior based on Fig. 5(a). The first part of all curves roughly is linear up to yield point (i.e. Y), when the steel bars on the tension face yielded. The secant stiffness and yield strength are improved with increasing longitudinal stiffness of the FRP. Beyond the yield point, the FRP are effectively activated,

so the second part of all curves continues although at a stiffness that is lower than that for the elastic region. The tangent stiffness at plastic region is improved with increasing longitudinal stiffness of the FRP. The maximum load carrying of each specimen is achieving at FRP failure point (i.e. F), that the FRP is broken. For example, the failure force of S300-L4T is equal to 354 kN, which shows a 127% increase beyond the unstrengthened specimen (i.e. U300). Table 3 shows longitudinal secant stiffness, yield point, longitudinal tangent stiffness, and failure point of all specimens.

The load-displacement curves of specimens with 200 mm eccentricity are shown in Fig. 5(b). The overall behavior of unstrengthened specimen (i.e. U200) is similar to U300. There is a difference in failure mode of U200 that shows limited plastic region and softening behavior because of buckling of compression steel bars at peak load. The strengthened specimens have bilinear behavior similar to previously discussed strengthened specimens. Based on Fig. 5 and failures observation, failure of the strengthened specimens is governed by rupture of the longitudinal layers at the tension face, that means the balance point is not reached and all of the specimens failed in tension-controlled failure.

Moment-Curvature Behavior

Figures 6(a) and (b) show the moment-curvature behavior of the specimens at the mid height of the test length. The bending moment M was calculated with multiplying the load P by actual eccentricity as shown in Eq. (1). The actual eccentricity was determined at each load step by predefined eccentricity e plus mid height deflection U_{Lat} at the previous load step. Thus the bending moments were evaluated considering second order effects.

$$M = P\left(e + U_{Lat}\right) \tag{1}$$

The curvature φ was obtained using the differential longitudinal strain on the top and bottom fasces of mid height section based on the plane section assumption, as the follows:

$$\phi = \frac{\varepsilon_{L,top} - \varepsilon_{L,bot}}{h} \quad (2)$$

where $\varepsilon_{L,top}$ is longitudinal strain of top face and $\varepsilon_{L,bot}$ is longitudinal strain of bottom face of mid height section; and h is the height of section (i.e. 300 mm) as shown in Fig. (6).

It is shown that longitudinal layers improved bending stiffness and moment capacity of the specimens, but curvature capacities are not generally improved. The moment-curvature behavior of the specimen with DD' fiber orientation is a little different because it almost shows an elasto-plastic behavior. In this case, not only bending stiffness and moment capacity are enhanced, but also curvature capacity is improved. This special effect of angle orientation (i.e. DD') has been significantly observed in axial compressive tests of CFRP confined concrete cylinders and axial tensile tests of CFRP coupons by the authors (Sadeghian et al. 2008 and 2009). The ductility improvement is produced by plastic shear behavior of resin in FRPs with diagonal fibers. In case of specimen S300-DD', because of the rectangular section and eccentric loading, the improvement of the angle orientation on ductility has been limited.

Longitudinal and Transverse Strains

Figures 7(a) and (b) show the variation of longitudinal strain $\varepsilon_{L,bot}$ and transverse strain $\varepsilon_{T,bot}$ on the bottom face (i.e. compression face) of the specimens at the mid height section. The behavior of the unstrengthened specimens (i.e. U200 and U300) expresses that the maximum longitudinal strain (i.e. at the failure point) of both specimens is almost 2.6 mm/m (on compression face) which is compatible with the ultimate strain of plain concrete in compression. The maximum longitudinal strains of the strengthened specimens on compression face (i.e. where the longitudinal fibers are compressed) are almost the same and equal to 2.6 mm/m. Thus the transverse fibers could not make any improvement on the

confinement of the compression side of the section, when the columns are failed in tension-controlled failure.

Figures 8(a) and (b) show the variation of longitudinal strain $\varepsilon_{L,top}$ and transverse strain $\varepsilon_{T,top}$ on the top face (i.e. tension face) of the specimens at the mid height section. The behavior of the unstrengthened specimens (i.e. U200 and U300) expresses that the average maximum strain on the tension face is 6 mm/m, so the steel bars (ε_y =2.3 mm/m) on the tension face have yielded. Based on the failure points of the strengthened specimens, the average maximum longitudinal strain of the FRP (in fiber direction) is 5.9 mm/m. The coupon test results (Table 2) show that the ultimate strain of the FRP in fiber direction is 7.4 mm/m. This difference is logical, because the FRP on the large-scale specimens is not in a unidirectional stress condition contrary to the coupon tests condition.

Figures 7 and 8 show that the highest transverse strains of all specimens happen on the compression side (i.e. where concrete expands) rather than on the tension side (i.e. where concrete contracts, as it is expected. In case of the strengthened specimens, the maximum transverse strains on compression face (Fig. 7) for eccentricity of 200 and 300 mm are averagely 0.5 and 0.3 mm/m, respectively. In comparison with the ultimate strain of the FRP in fiber direction (Fig. 8 and Table 2), it shows that in tension-controlled failures, the transverse layers are not activated fully and the effects of confinement are limited.

Lateral Deformation

The lateral displacements recorded by the lateral LVDT1 to LVDT5 are presented in Fig. 9, when the lateral displacement at mid height section (i.e. LVDT3) is 5, 10, 15, and 20 mm for all of the specimens. The displacements recorded by the corresponding upper and lower LVDTs had a little difference, so the corresponding values have been averaged. It is

mentioned that at the same lateral displacement, each specimen presents a totally different axial load.

The lateral deformation is induced under a combination of initial moment and second order moment as Eq. (1). For design calculations of ordinary pinned RC columns under second order deformation, a sine-shaped deformation is often assumed (Lloyd and Rangan 1996; Claeson and Gylltoft 1998):

$$\delta = \Delta \sin\left(\frac{\pi x}{\mathrm{L}}\right) \tag{3}$$

where Δ is the maximum lateral displacement at mid height section, x is longitudinal coordinate variable, L is length of the pinned column, and δ is the lateral displacement at x position as Fig. 9. The performance of the model against the experimental data and average curve of them is presented in Fig. 9. The figure demonstrates that the model has a very good agreement with the experimental data on the constant cross section of 200 mm × 300 mm (i.e. on the middle prismatic column). This model is good prediction for different level of deformation from linear region up to failure point. Thus the sine-shaped model of ordinary RC columns can be used for RC columns strengthened with CFRP composites.

Conclusion

In an attempt to explain the behavior of RC rectangular concrete column strengthened with CFRP composites under eccentric loading, seven large-scale specimens (200mm × 300mm × 2700 mm) with haunched heads were prepared and subjected to eccentric compression loading up to failure. The various parameters such as FRP thickness, fiber orientation, and eccentricity were considered. The effects of these parameters on load-displacement and moment-curvature behavior as well as the variation of longitudinal and lateral strains on compression and tension faces of the specimens were studied. The following conclusions are drawn:

1. The strengthened specimens had similar bilinear load-displacement curves as unstrengthened specimens. The first part of all curves was approximately linear up to yield point, when the tension steel bars yielded. Axial secant stiffness and yield strength were improved with increasing axial stiffness of the FRP. After yielding point, the FRP were effectively activated, so the plastic region of all curves had limited stiffness degradation. The axial tangent stiffness was improved with increasing longitudinal stiffness of the FRP. The maximum load carrying capacity of each specimen was reached at FRP failure point, when the longitudinal fibers of FRP failed in tension.
2. The moment-curvature behavior showed that longitudinal layers improved bending stiffness and moment capacity of the specimens, but curvature capacities were not generally improved. The behavior of the specimen with angle orientation was a little different. In this case, not only bending stiffness and moment capacity were enhanced, but also curvature capacity was improved.
3. When the strengthened columns fail in tension-controlled failure, the transverse layers could not make any improvement on the confinement of the compression side of the section. In this region the concrete behavior is similar to unconfined concrete.
4. The sine-shaped model for second order deformation is in a good agreement with experimental data for different levels of deformation from linear region up to failure point, on prismatic part of the specimens. The model can be used for design calculation of RC columns strengthened with CFRP composites.

Acknowledgements

The authors wish to acknowledge the financial support provided by the Amirkabir University of Technology (Tehran Polytechnic). The Authors are grateful to Dr. T. Taghikhani, Dr. F.

Hatami, Mr. M.S. Khaleghi Moghaddam, Mr. A. Nikookar, Mr. A. Rajabi, and Mr. A. Aminabadi (Ostad Asghar) for their efforts and assists during this experimental research.

Notation

The following symbols are used in this paper:

d = distance between load cell and LVDT0;

e = eccentricity;

f_c' = compressive strength of concrete;

f_y = yielding strength of steel bars;

L = length of column;

M = bending moment;

P = axial load;

U_{Lon} = longitudinal displacement;

U_{Lat} = lateral displacement at mid height section;

x = longitudinal coordinate variable;

δ = lateral deformation;

Δ = maximum lateral deformation;

$\varepsilon_{L,bop}$ = longitudinal strain on bottom face;

$\varepsilon_{L,top}$ = longitudinal strain on top face;

$\varepsilon_{T,bot}$ = transverse strain on bottom face;

ε_y = yielding strain of steel bars; and

φ = curvature.

References

1. Chaallal, O., and Shahawy, M. (2000). “Performance of fiber-reinforced polymer-wrapped reinforced concrete column under combined axial-flexural loading.” *ACI Struct. J.*, 97(4), 659–688.
2. Claeson, C., and Gylltoft, K. (1998). “Slender high-strength concrete columns subjected to eccentric loading.” *J. Struct. Engrg.*, 124(3), 223–240.
3. Fam, A., Flisak, B., and Rizkalla, S. (2003). "Experimental and analytical modeling of concrete-filled fiber-reinforced polymer tubes subjected to combined bending and axial loads." *ACI Struct. J.*, 100(4), 1–11.
4. Hadi, M. N. S. (2006a). “Behaviour of FRP wrapped normal strength concrete columns under eccentric loading.” *Compos. Struct.*, 72(4), 503–511.
5. Hadi, M. N. S. (2006b). “Comparative study of eccentrically loaded FRP wrapped columns.” *Compos. Struct.*, 74(2), 127–35.
6. Hadi, M. N. S. (2007a). “Behaviour of FRP strengthened concrete columns under eccentric compression loading.” *Compos. Struct.*, 77(1), 92–96.
7. Hadi, M. N. S. (2007b). “The behaviour of FRP wrapped HSC columns under different eccentric loads.” *Compos. Struct.*, 78(4), 560–566.
8. Hadi, M. N. S., and Li, J. (2004). “External reinforcement of high strength concrete columns.” *Compos. Struct.*, 65(3–4), 279–287.
9. Li, J., Hadi, and M. N. S. (2003). “Behaviour of externally confined high strength concrete columns under eccentric loading.” *Compos. Struct.*, 62(2), 145–153.
10. Lignola, G. P., Prota, A., Manfredi, G., Cosenza, E. (2007). “Experimental performance of RC hollow columns confined with CFRP.” *J. Compos. Constr.*, 11(1), 42–49.
11. Lloyd, N. A., and Rangan, B. V. (1996). “Studies on high-strength concrete columns under eccentric compression.” *ACI Struct. J.*, 93(6), 631–638.

12. Parvin A., and Wang, W. (2001). "Behaviour of FRP jacketed concrete columns under eccentric loading." *J. Compos. Constr.*, 5(3), 146–152.
13. Sadeghian, P., Rahai, A. R., and Ehsani, M. R. (2009). "Effect of fiber orientation on nonlinear behavior of CFRP composites." *J. of Reinforced Plastics and Compos.*, 28(18), 2261–2272.
14. Sadeghian, P., Rahai, A. R., and Ehsani, M. R. (2009). "Effect of fiber orientation on compressive behavior of CFRP-confined concrete columns." *J. of Reinforced Plastics and Compos.*, Online Published on July 2 as doi: 10.1177/0731684409102985.
15. Yuan, X. F., Lam, L., Teng, J. G., and Smith, S. T. (2001). "FRP-confined RC columns under combined bending and compression: a comparative study of concrete stress–strain models." *Proc., Int. Conf. on FRP composites in civil engineering, 12–15 December, Hong Kong, China,* 749–758.

Table 1. Specimen design details

Specimen	Strengthening	Number of layers	Fiber orientation	Eccentricity (mm)
U200	Unstrengthened	-	-	200
U300	Unstrengthened	-	-	300
S200-L2T	Strengthened	3	$(90^o)_2/0^o$	200
S200-L4T	Strengthened	5	$(90^o)_4/0^o$	200
S300-L2T	Strengthened	3	$(90^o)_2/0^o$	300
S300-L4T	Strengthened	5	$(90^o)_4/0^o$	300
S300-DD'	Strengthened	2	$\pm 45^o$	300

Table 2. Mechanical properties of CFRP coupon (Sadeghian et al. 2008)

Test direction	Ultimate strength (MPa)	Initial modulus (MPa)	Ultimate strain (mm/m)	FRP thickness (mm/layer)	Dry thickness (mm/layer)
Fiber direction	303	41000	7.4	0.9	0.25
Matrix direction	29	2400	7.2	0.9	0.25

Table 3. Experimental results

Specimen	Longitudinal secant stiffness (kN/mm)	Yield Point		Longitudinal tangent stiffness (kN/mm)	FRP failure point	
		Load (kN)	U_{Lon} (mm)		Load (kN)	U_{Lon} (mm)
U200	40.9	303	7.4	11.3	337	10.4
U300	19.7	128	6.5	1.8	156	22.0
S200-L2T	40.5	401	8.2	20.0	491	12.7
S200-L4T	58.8	482	8.2	29.5	600*	12.2*
S300-L2T	24.1	195	8.1	12.5	284	15.2
S300-L4T	28.0	294	10.5	16.8	356	14.2
S300-DD'	18.3	163	8.9	4.4	238	25.9

* The FRP did not fail because of the limitation of the actuator capacity

Figure 1

Click here to download high resolution image

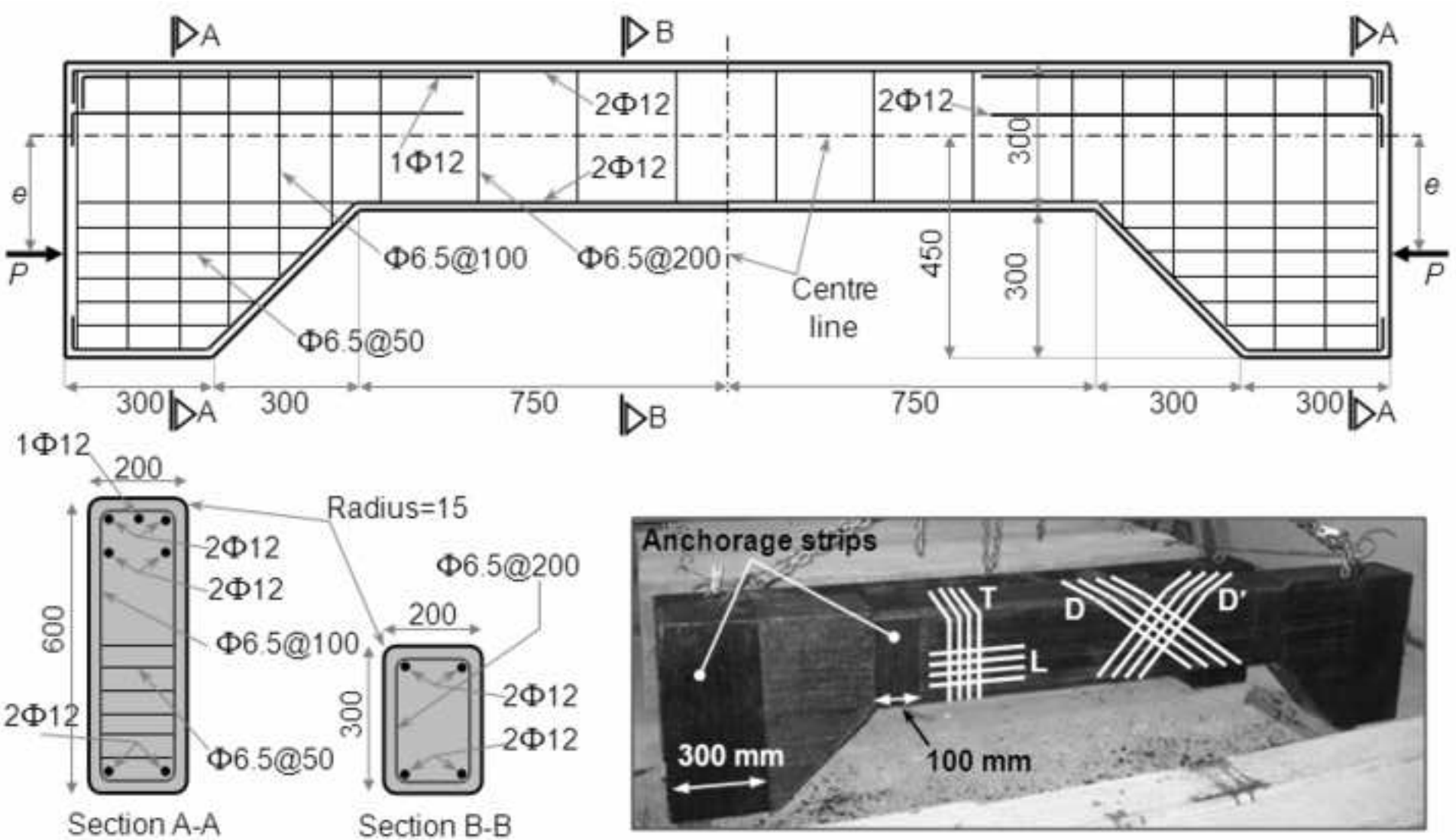

Figure 2

Click here to download high resolution image

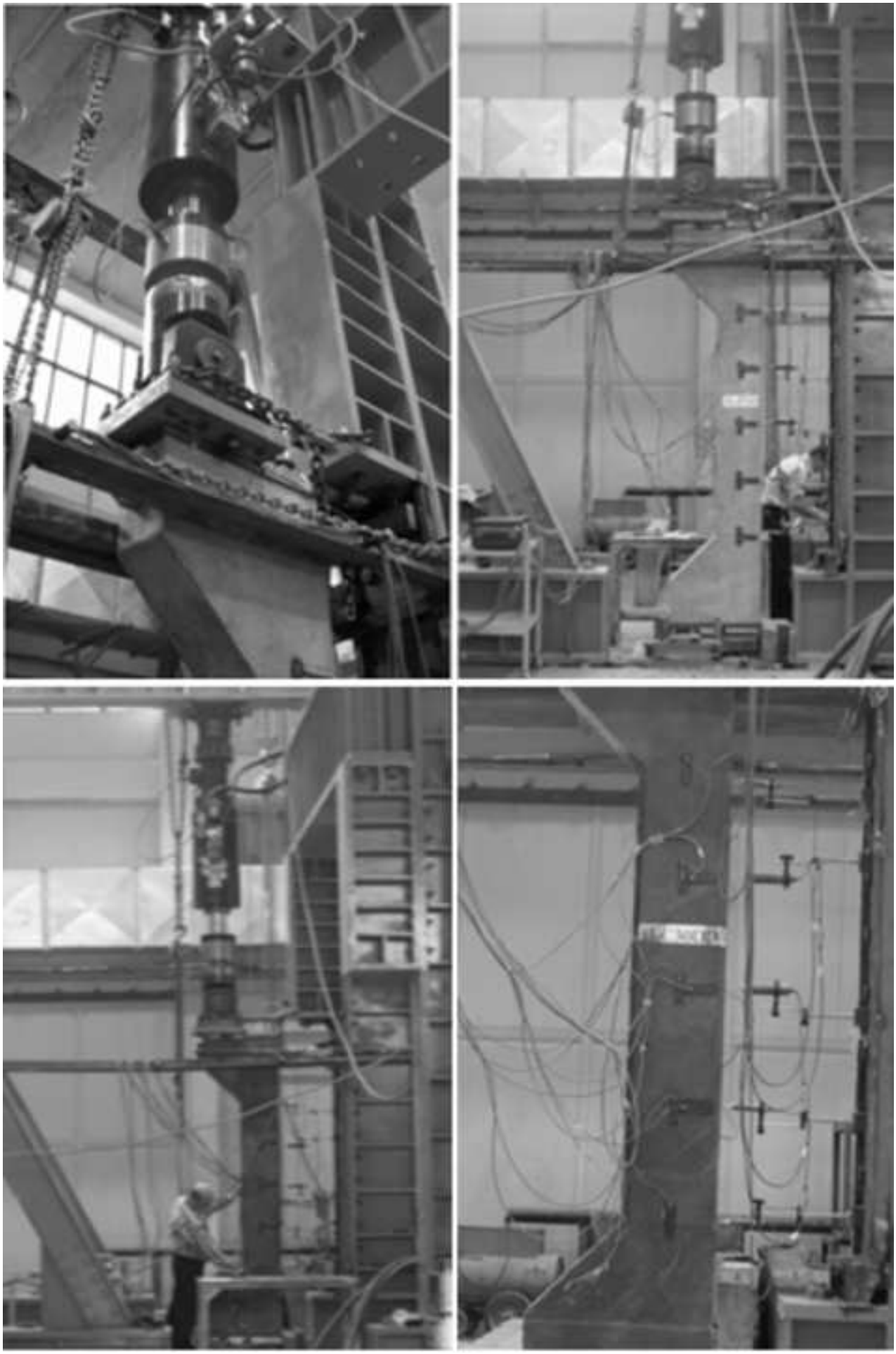

Figure 3

Click here to download high resolution image

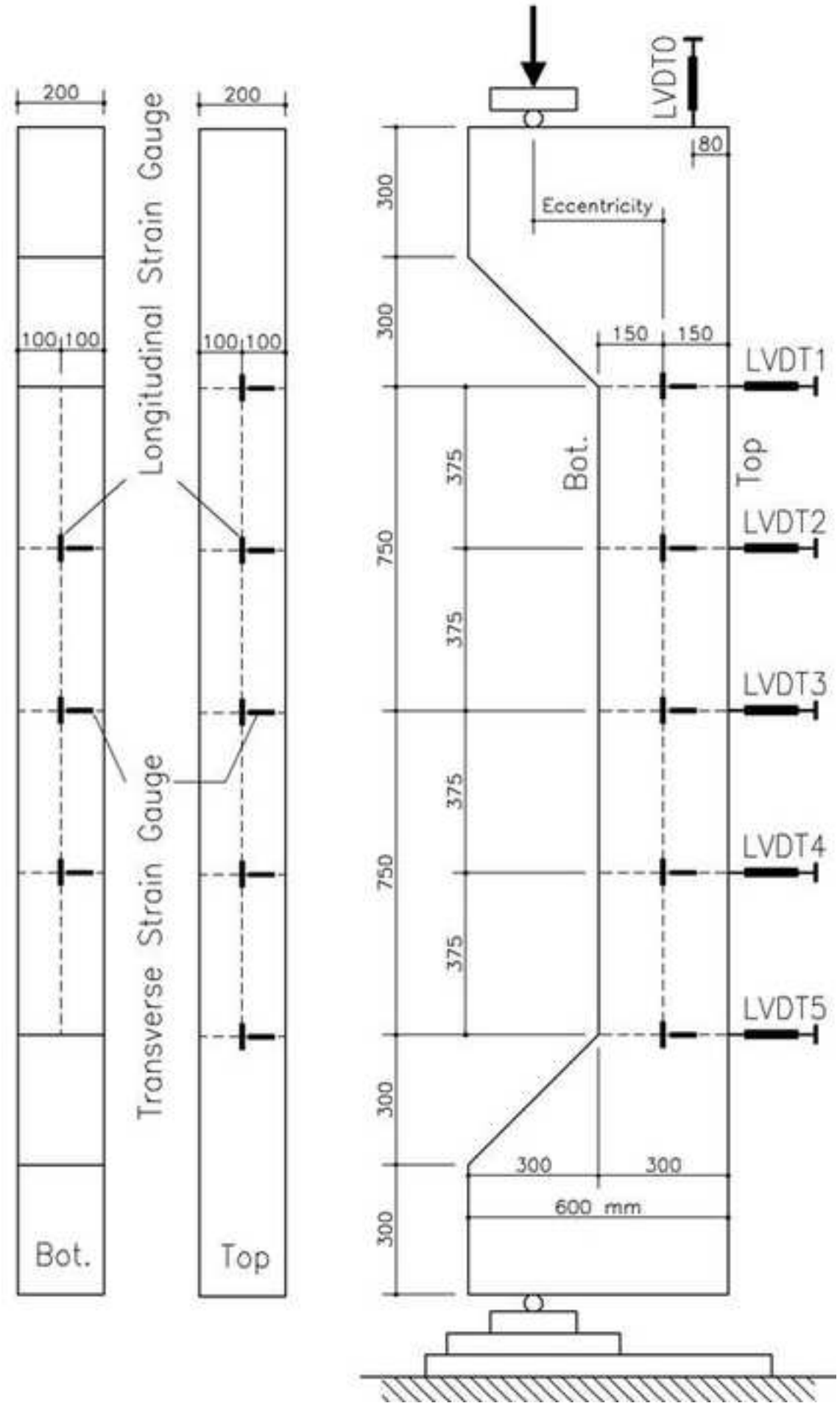

Figure 4

Click here to download high resolution image

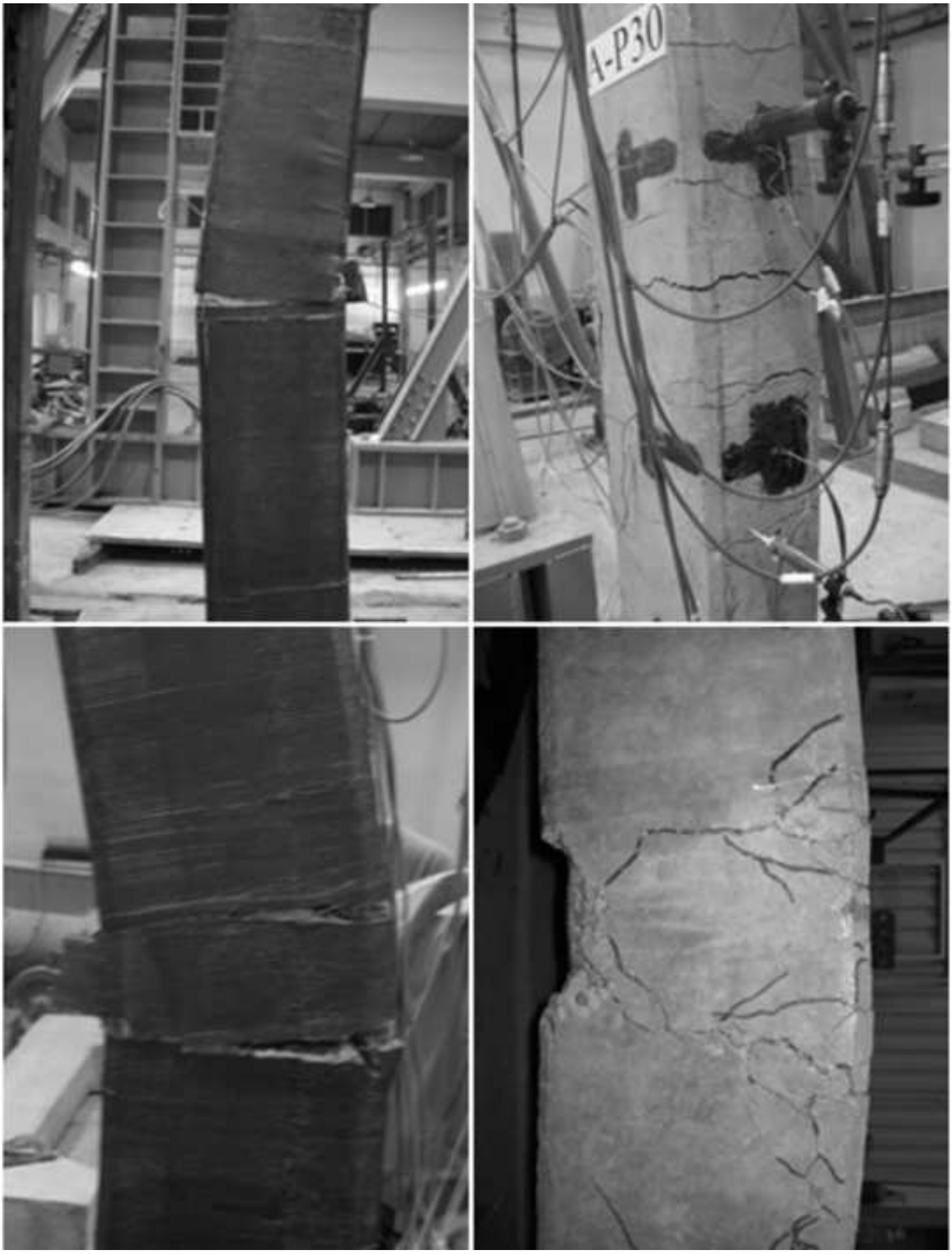

Figure 5a

Click here to download high resolution image

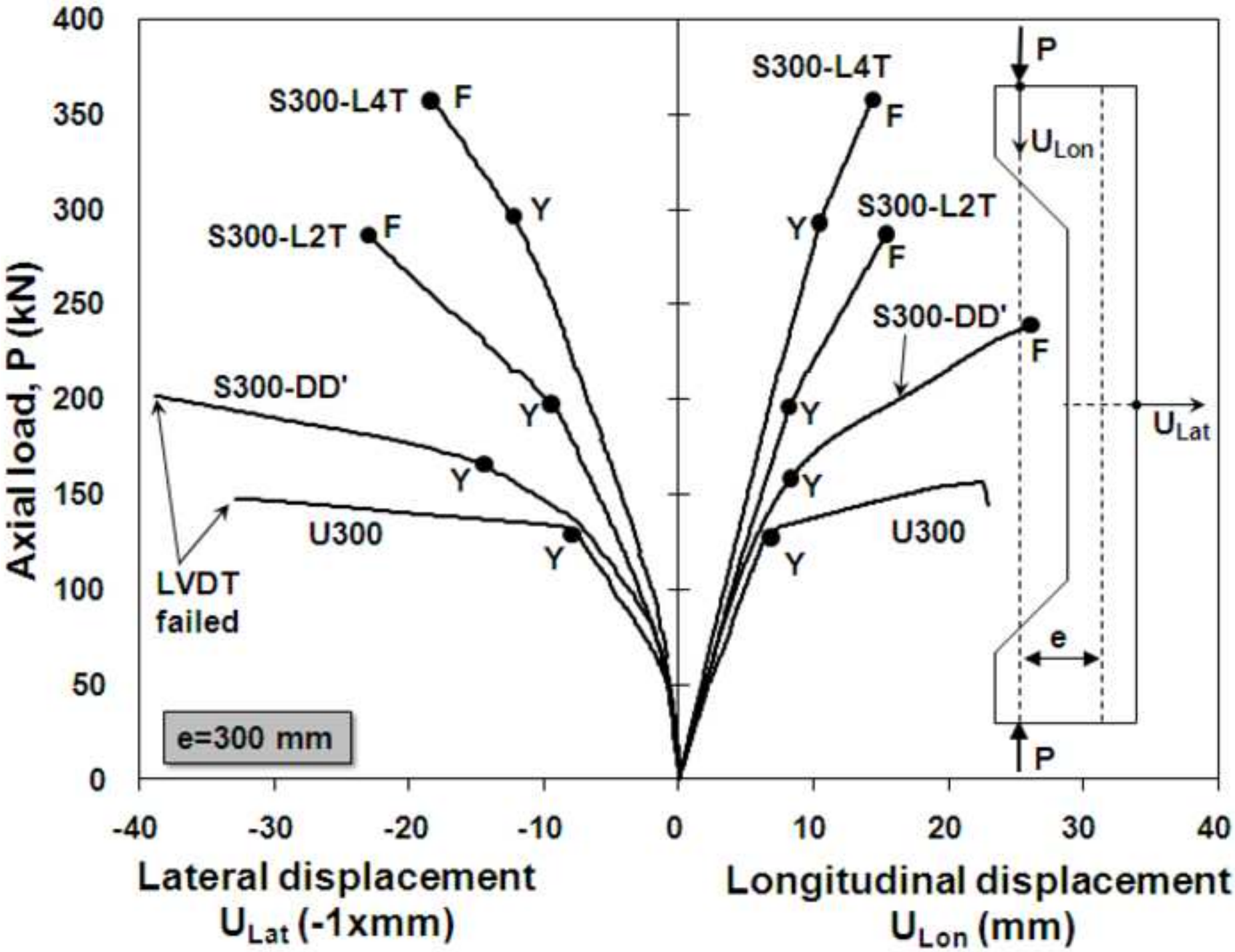

Figure 5b

Click here to download high resolution image

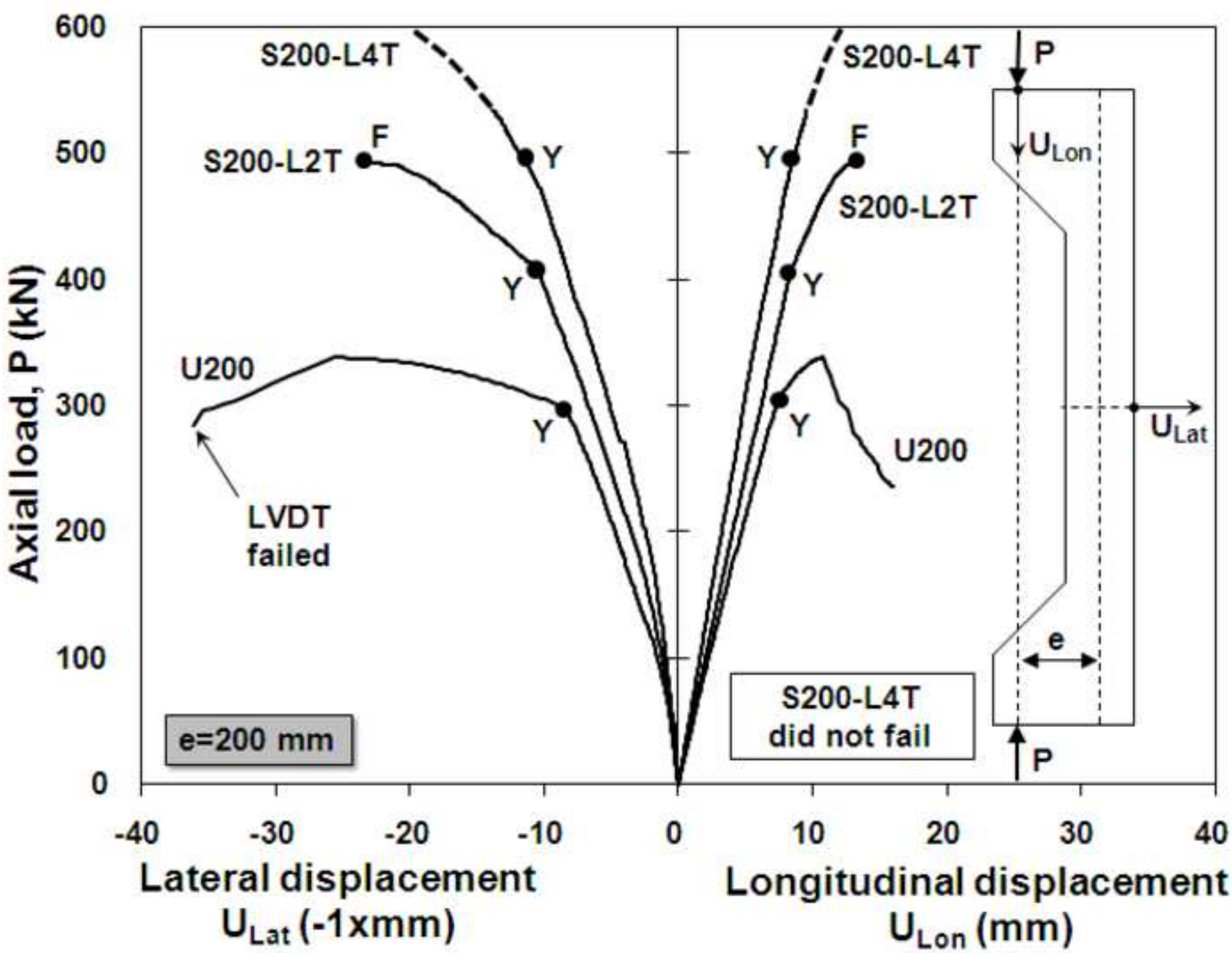

Figure 6a

Click here to download high resolution image

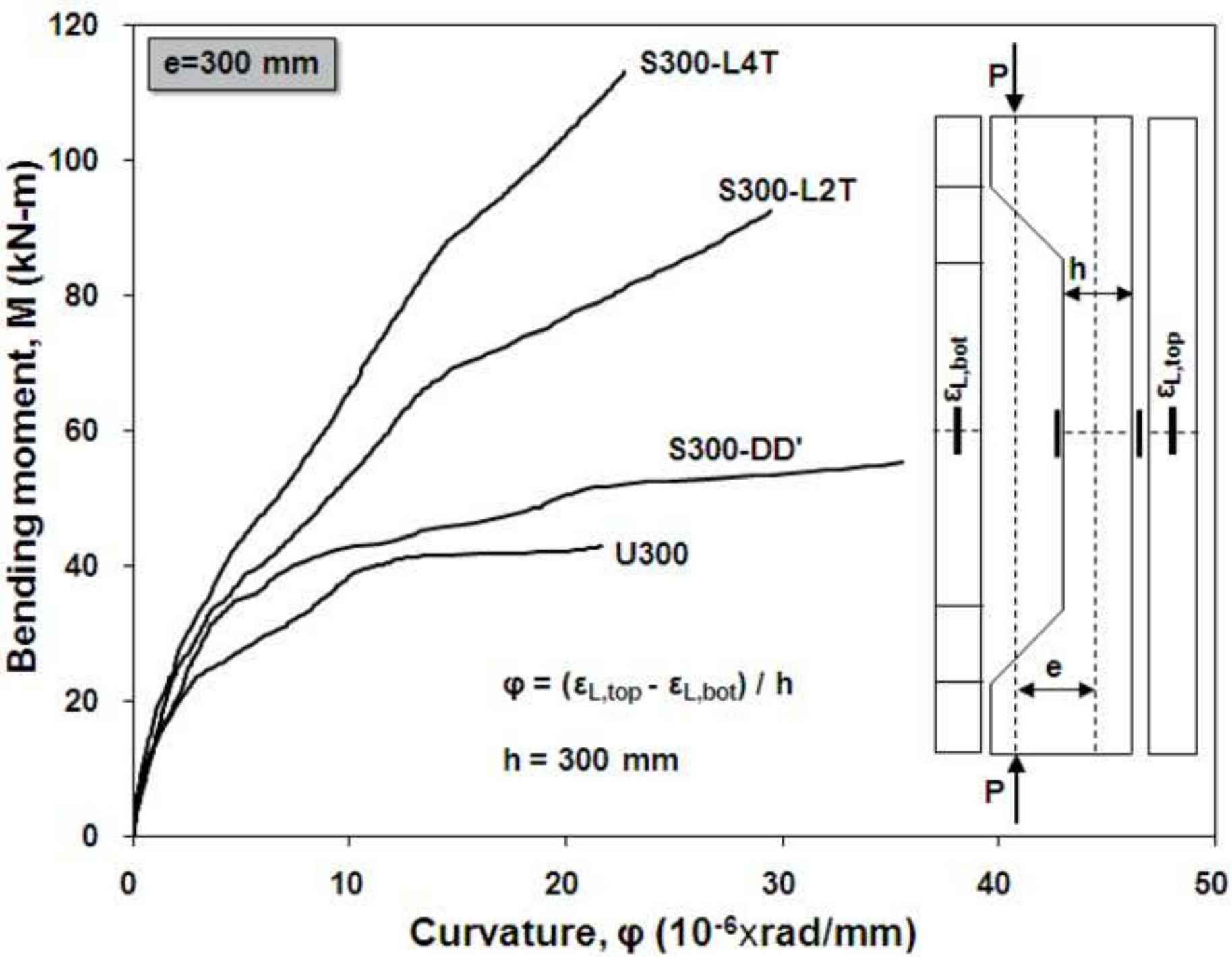

Figure 6b

Click here to download high resolution image

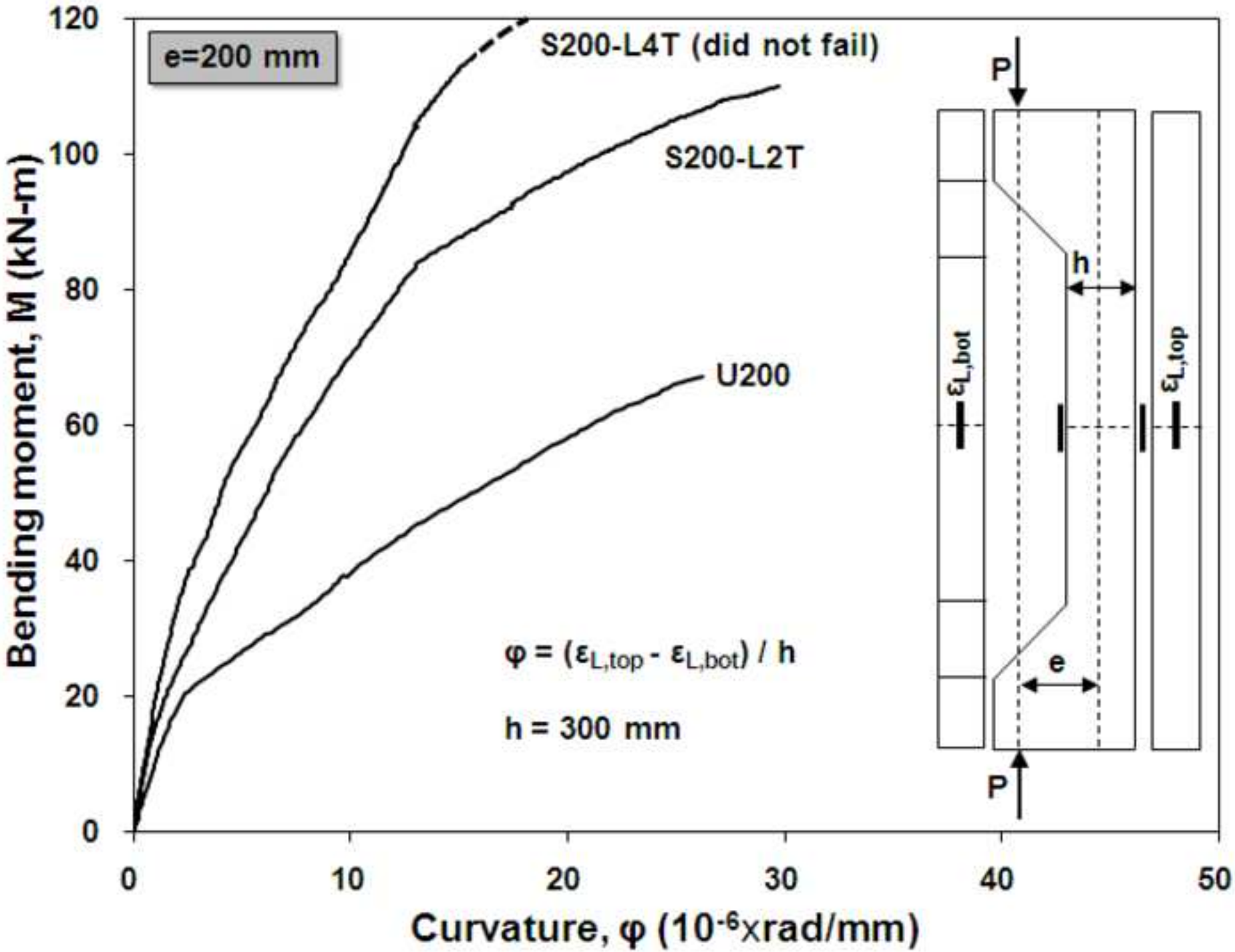

Figure 7a

Click here to download high resolution image

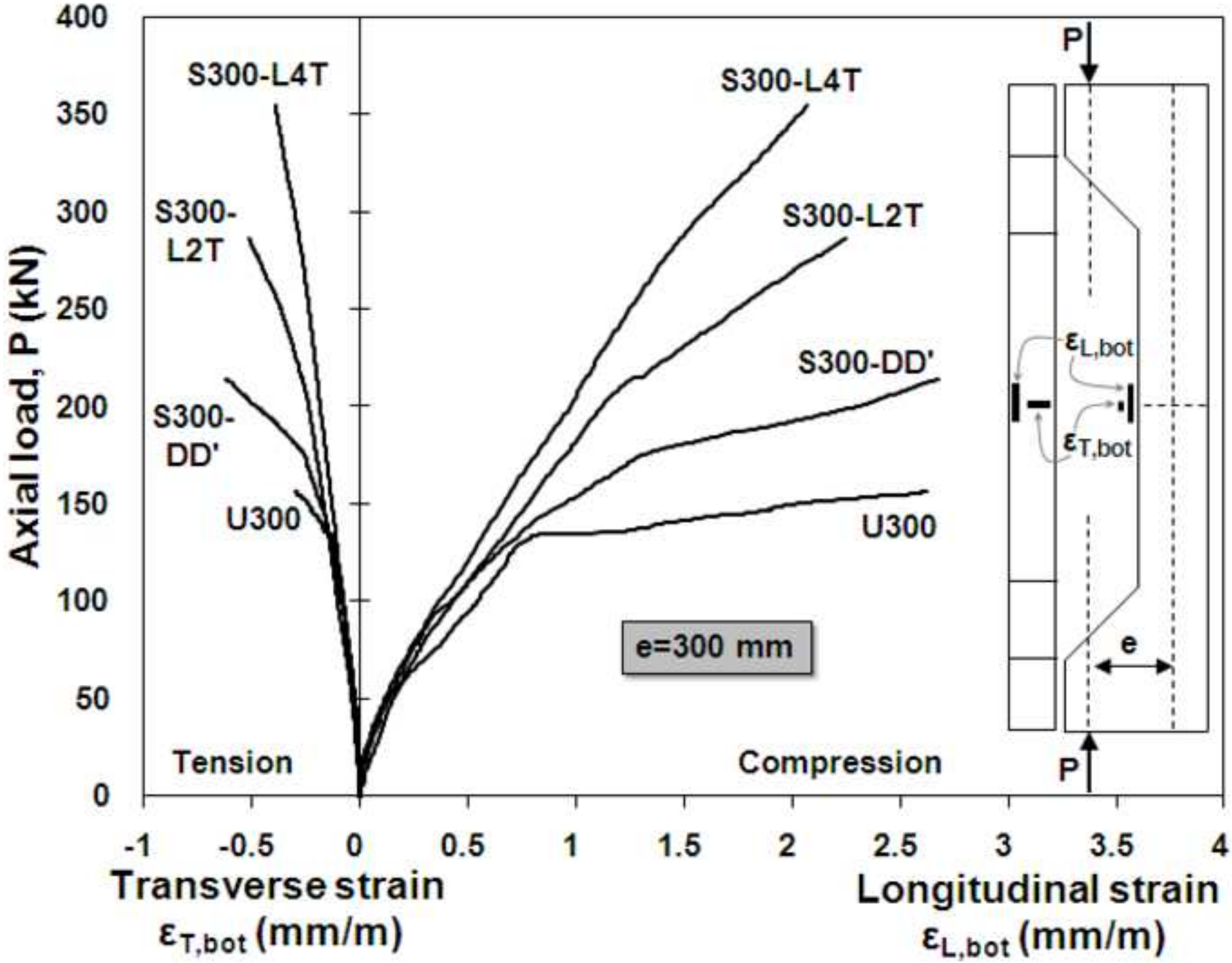

Figure 7b

Click here to download high resolution image

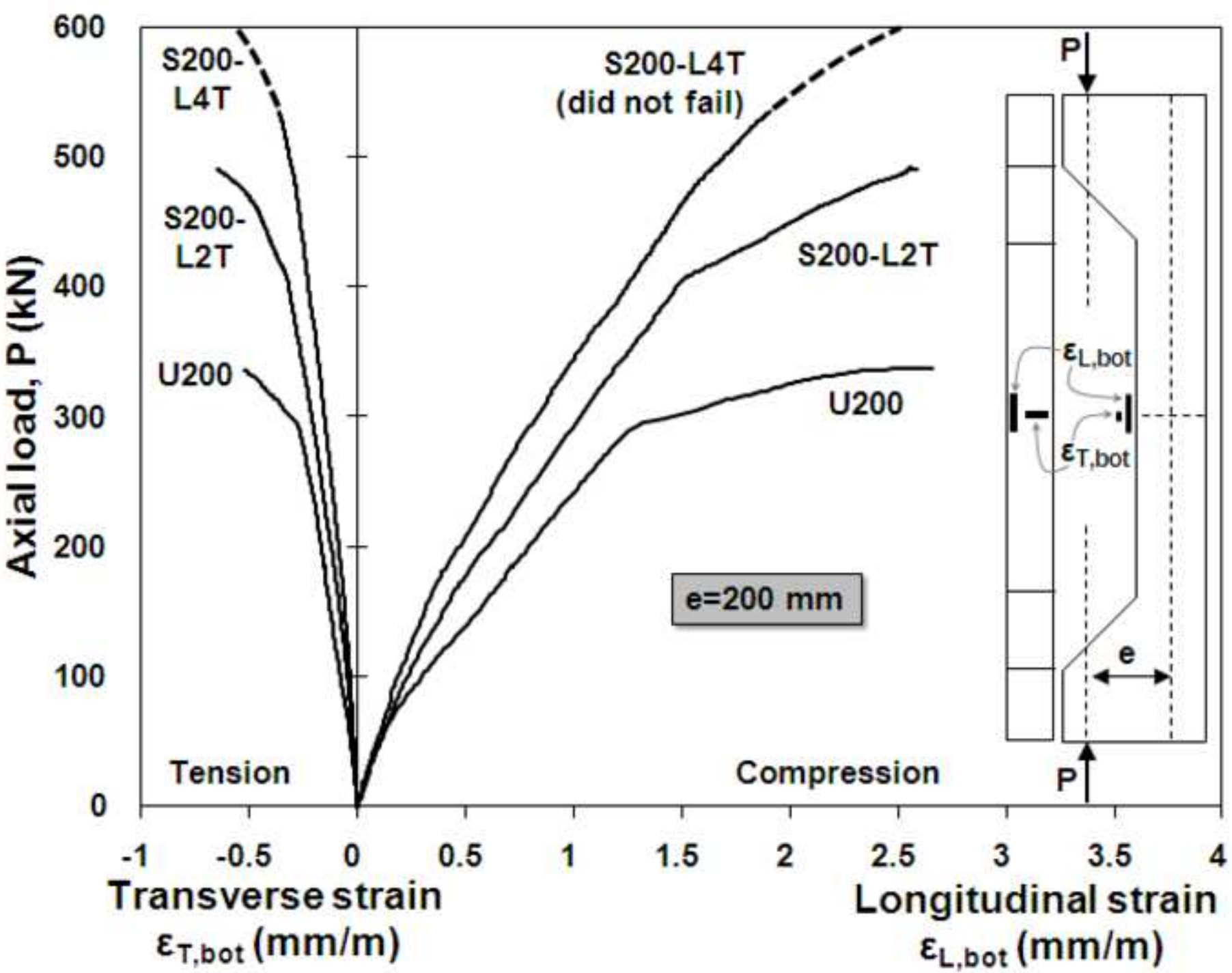

Figure 8a

Click here to download high resolution image

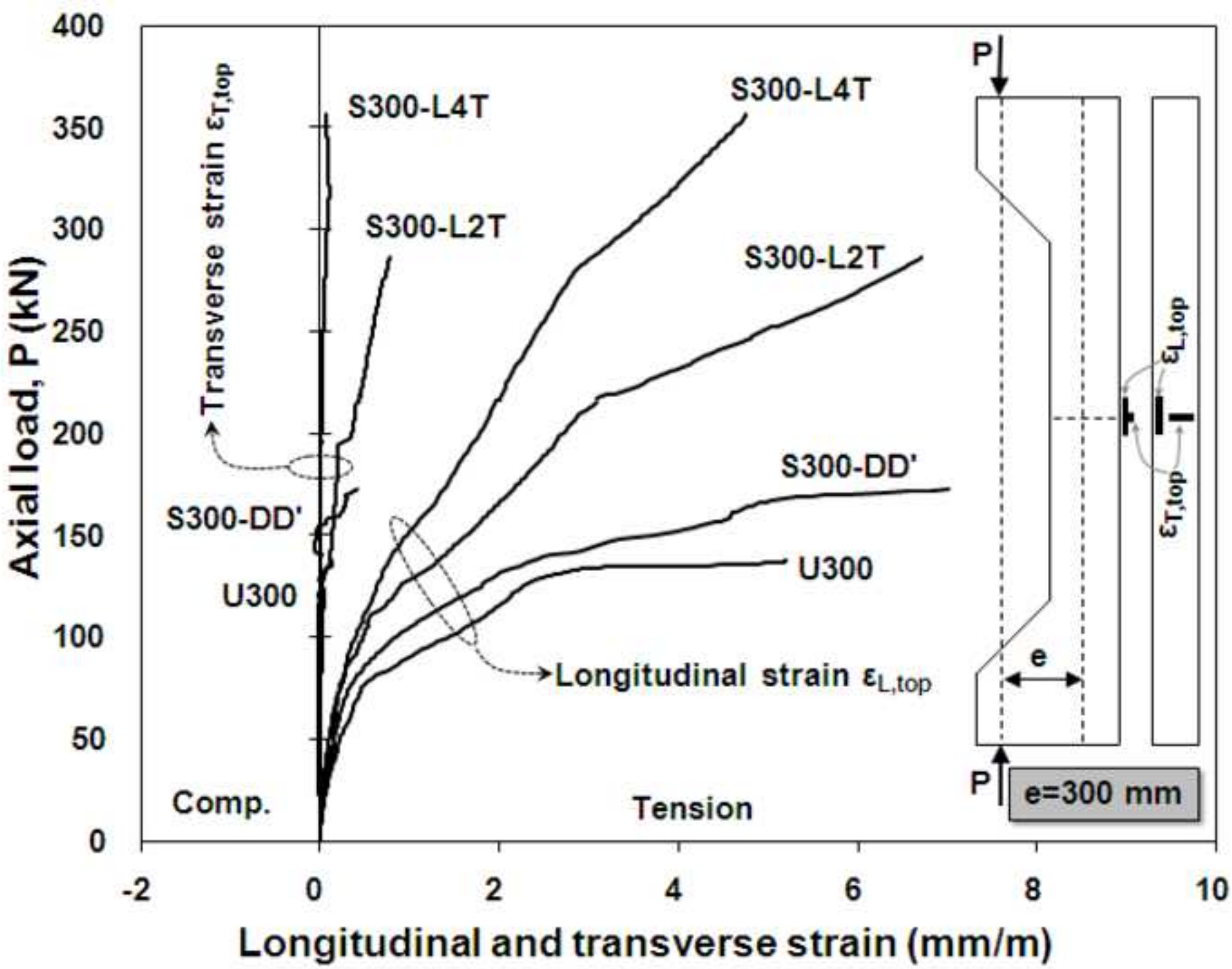

Figure 8b

Click here to download high resolution image

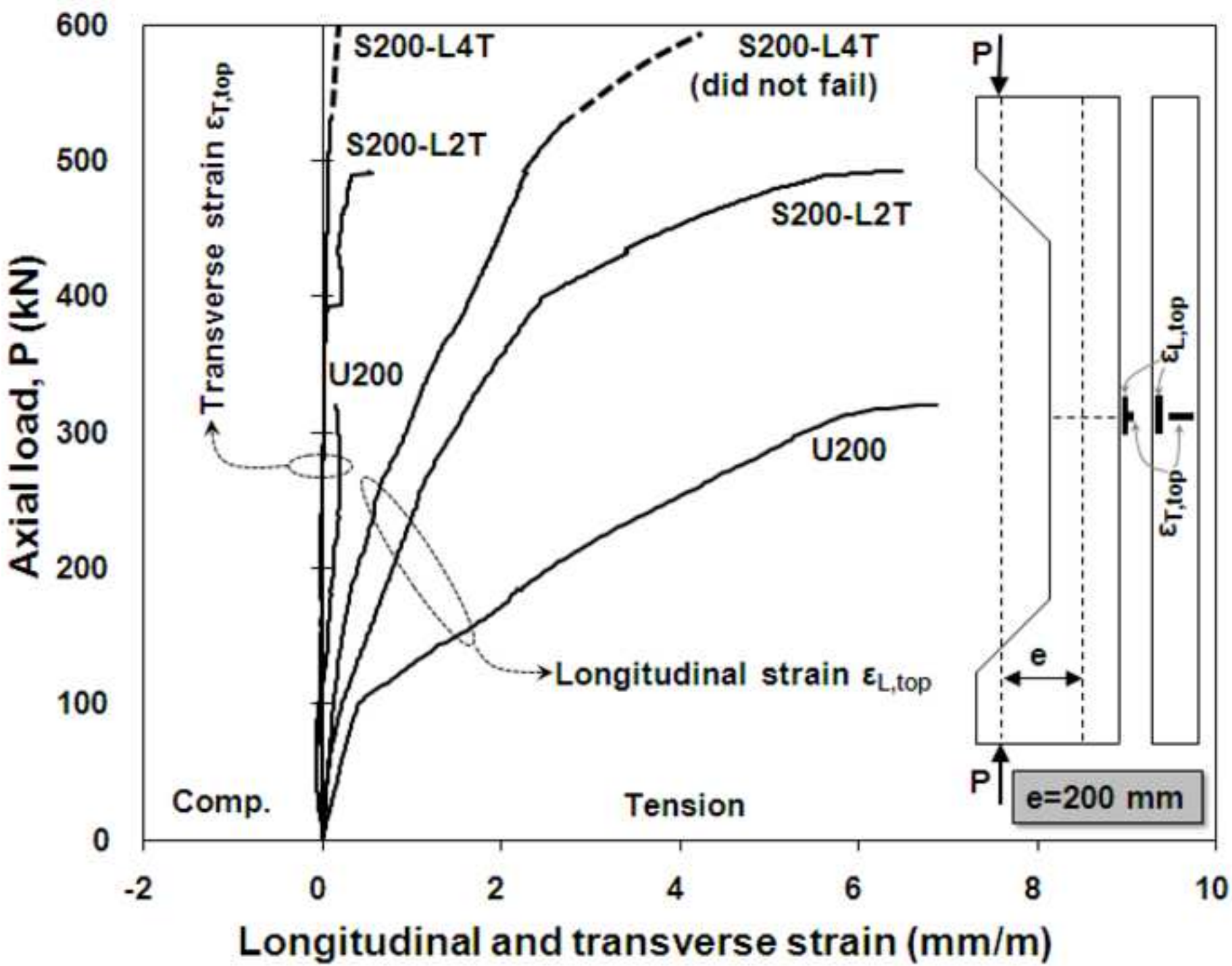

Figure 9

Click here to download high resolution image

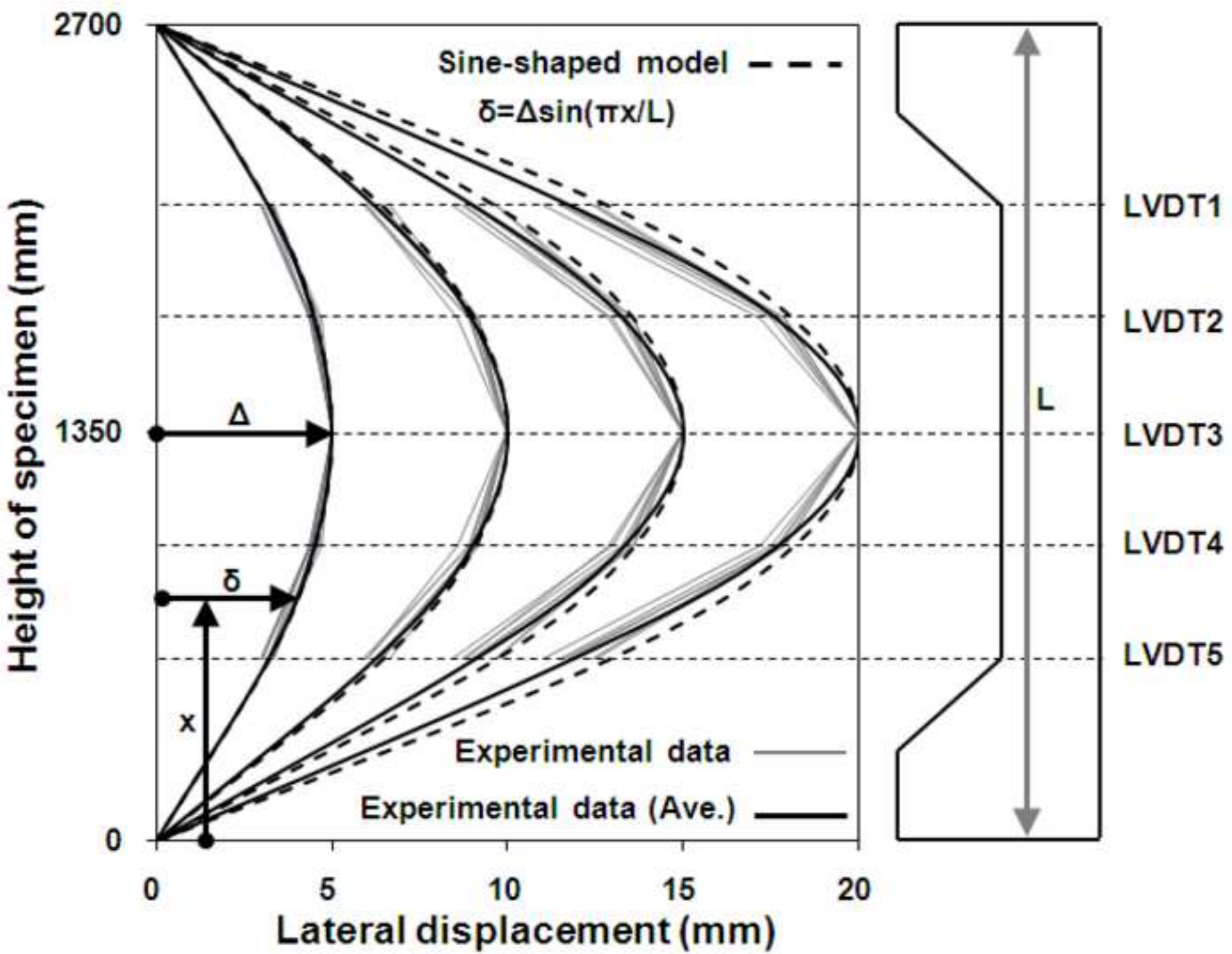

Figure Captions List